Article

RAN potentiates nuclear export of phosphorylated AMPK, reshaping lipid metabolism and impairing immune efficacy in lung adenocarcinoma

Check for updates

Qingwu Du[1,2,3,4,5], Rui Li[1,2,3,5], Jian Wang[1,2,3,5], Jingya Wang[1,2,3,4], Yantao Jiang[1,2,3,4], Qi Xu[1,2,3,4], Dingzhi Huang[1,2,3,4] ✉ & Tingting Qin[1,2,3,4] ✉

The therapeutic effectiveness of immune checkpoint inhibitors (ICIs) in lung cancer remains constrained and demonstrates substantial variability across different patients. Targeting the metabolism of tumors emerges an encouraging strategy to enhance the outcomes of tumor immunotherapy. We analyzed metabolic differences in lung cancer post-anti-PD-1 treatment using a single-cell RNA sequencing data ($n = 15$). Abnormal lipid metabolism is notable in patients with a non-major pathological response, and low RAN expression is linked to good immunotherapy response. RAN showed increased expression in lung adenocarcinoma (LUAD) versus normal lung tissues, correlating with worse prognosis, advanced staging, reduced immune cell activity, and greater sensitivity to common chemotherapeutic drugs. Knockdown of RAN caused G2/M phase arrest, inhibiting proliferation and clone formation in LUAD cells. RAN modifies lipid metabolism via nuclear p-AMPK output to aid tumor cells in resisting immunotherapy and reduces MHC-related molecule expression to evade CD8 + T cell detection. Combining Selinexor with immunotherapy might effectively counter immune tolerance and boost anti-tumor responses in LUAD.

Lung adenocarcinoma (LUAD), the most common type of lung cancer and part of the non-small cell lung cancer (NSCLC) group, is a major cause of cancer deaths[1]. Immune checkpoint inhibitors (ICIs) have revolutionized NSCLC treatment, becoming the primary therapy. However, about 75% of patients remain immune-refractory, experiencing disease progression during or after treatment[2]. To tackle this critical issue, it's essential to understand immune silence mechanisms and identify precise biomarkers to improve ICI effectiveness.

Tumor cells are characterized by metabolic reprogramming[3,4], particularly in lipid metabolism, which meets their energy needs and triggers signaling pathways and epigenetic changes, aiding in metastasis and resistance to therapies[5]. For instance, aggressive tumor cells increase fatty acid uptake by overexpressing CD36, boosting their metastatic potential and treatment resistance[6,7]. Furthermore, they also create a hypoglycemic, high-fat microenvironment that promotes lipid uptake in stromal cells,

leading to immune dysfunction and helping tumors evade immune detection[8,9]. Besides directly inhibiting tumor progression, targeting lipid metabolism has also demonstrated the potential to bolster the effectiveness of immunotherapy against tumors[10,11].

Despite advances in understanding, many aspects of metabolic remodeling in tumors remain to be fully elucidated. This includes the pronounced metabolic heterogeneity observed across different tumor types and the adaptive changes in metabolic profiles that occur throughout various stages of tumor progression[12,13]. This study aims to elucidate the comprehensive landscape of metabolic reprogramming in tumors following immunotherapy, with the objective of identifying novel molecular markers that significantly impact the efficacy of immunotherapeutic interventions. These findings will provide innovative insights and a theoretical foundation for the development of combined immunotherapeutic strategies.

[1]Tianjin Medical University Cancer Institute and Hospital, National Clinical Research Center for Cancer, Tianjin, PR China. [2]Key Laboratory of Cancer Prevention and Therapy, Tianjin, PR China. [3]Tianjin's Clinical Research Center for Cancer, Tianjin, PR China. [4]Department of Thoracic Oncology, Tianjin Lung Cancer Center, Tianjin Cancer Institute & Hospital, Tianjin Medical University, Tianjin, PR China. [5]These authors contributed equally: Qingwu Du, Rui Li, Jian Wang. ✉e-mail: dingzhih72@163.com; shadowzlyy@163.com

THE HORMEL INSTITUTE
UNIVERSITY OF MINNESOTA

Results

Single-cell RNA-seq (scRNA-seq) analysis indicates abnormal lipid metabolism linked to immune response

We conducted a re-analysis of scRNA-seq data derived from 15 patients with NSCLC within an immunotherapy cohort. Samples were collected from tumor tissues of 3 pre-treatment baseline patients and 12 patients post anti-PD1 treatment, comprising 4 cases of major pathological responses (MPR) and 8 additional cases of non-major pathological responses (NMPR) (Fig. 1A). Using a clustering algorithm and cell markers, we identified 22 clusters representing ten cell types: endothelial cell, fibroblast, mast cell,

natural killer cell, plasma cell, epithelial cell, myeloid cell, B cell, neutrophil, and T cell (Fig. 1B, C, and Supplementary Fig. S1A). Our analysis found notable differences in cell type proportions between the MPR and NMPR groups. The MPR group had significantly more adaptive immune cells (T-cells, B-cells, plasma cells) and fewer innate immune cells (neutrophils, myeloid cells) compared to the NMPR group (Supplementary Fig. S1B, C).

We used the scMetabolism algorithm to analyze metabolic changes in tumors pre- and post-immunotherapy. Firstly, the metabolic landscapes of tumor cells (i.e. epithelial cells) in the control, MPR and NMPR groups were compared (Fig. 1D). The results showed that the tumor cells at baseline
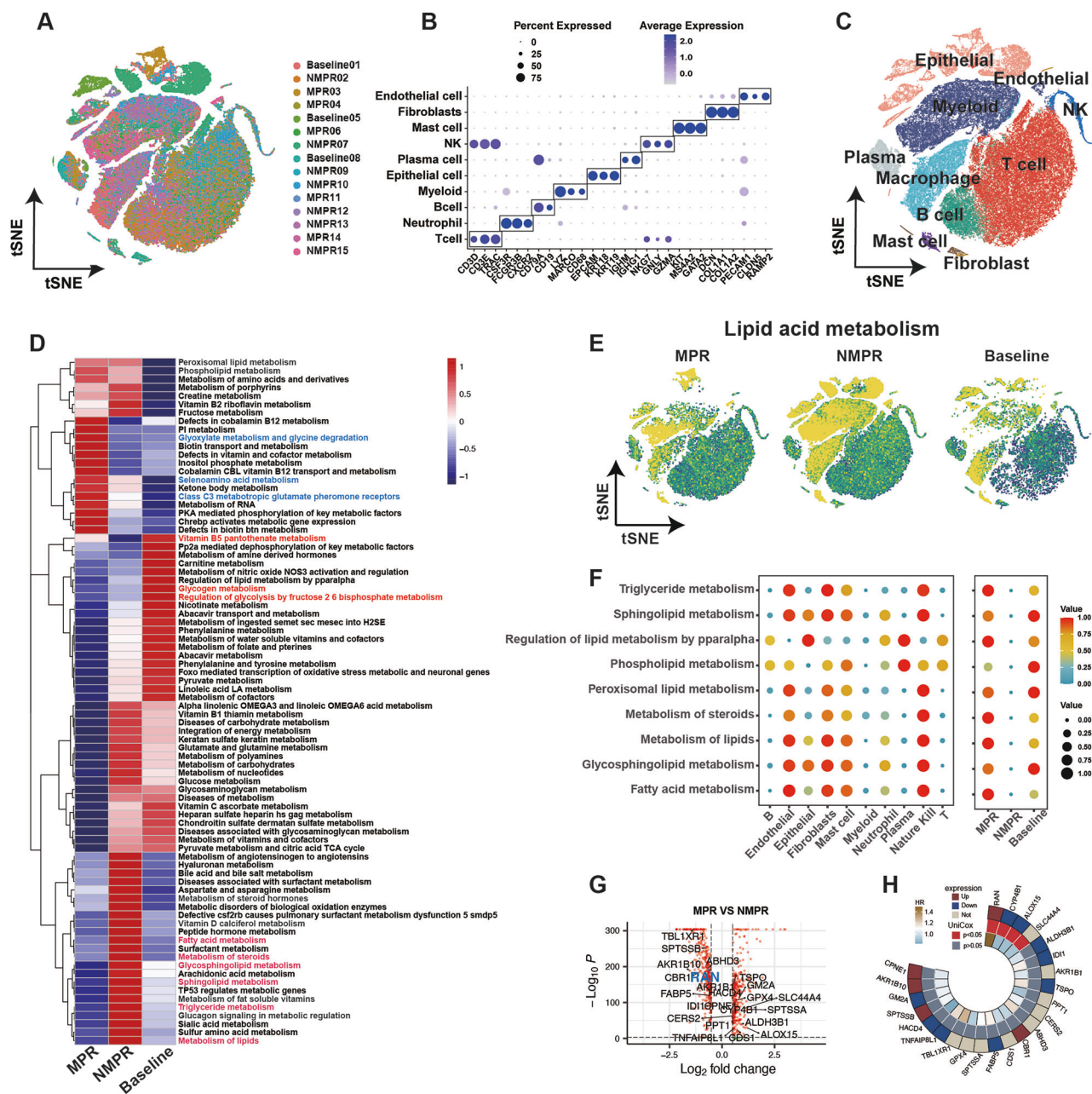
Fig. 1 | Cellular metabolic changes before and after Immunotherapy in LUAD. **A** The t-SNE map depicts 92,330 cells from 15 scRNA-seq samples. **B** A dot plot illustrates representative marker genes for each cell type. **C** The t-SNE map is colored based on cell-type annotation. **D** Metabolic pathway activities of tumor cells are compared before and after immunotherapy. **E** Distribution of the lipid acid metabolism score among cells in the baseline, MPR, and NMPR groups is shown. **F** A dot plot on the left displays metabolic characteristics of ten cell types from the NMPR group; on the right, a dot plot highlights metabolic characteristics of T cells across the baseline, MPR, and NMPR groups, with both color and size indicating the effect size. **G** A volcano plot identifies differentially expressed genes in the remaining tumor cells of the MPR and NMPR groups. **H** The Circos plot reveals 23 common genes from lipid metabolism gene sets and the aforementioned differentially expressed gene sets. Notably, five genes were upregulated in LUAD tumors compared to normal lung tissues in the TCGA cohort, and four genes were associated with overall survival.
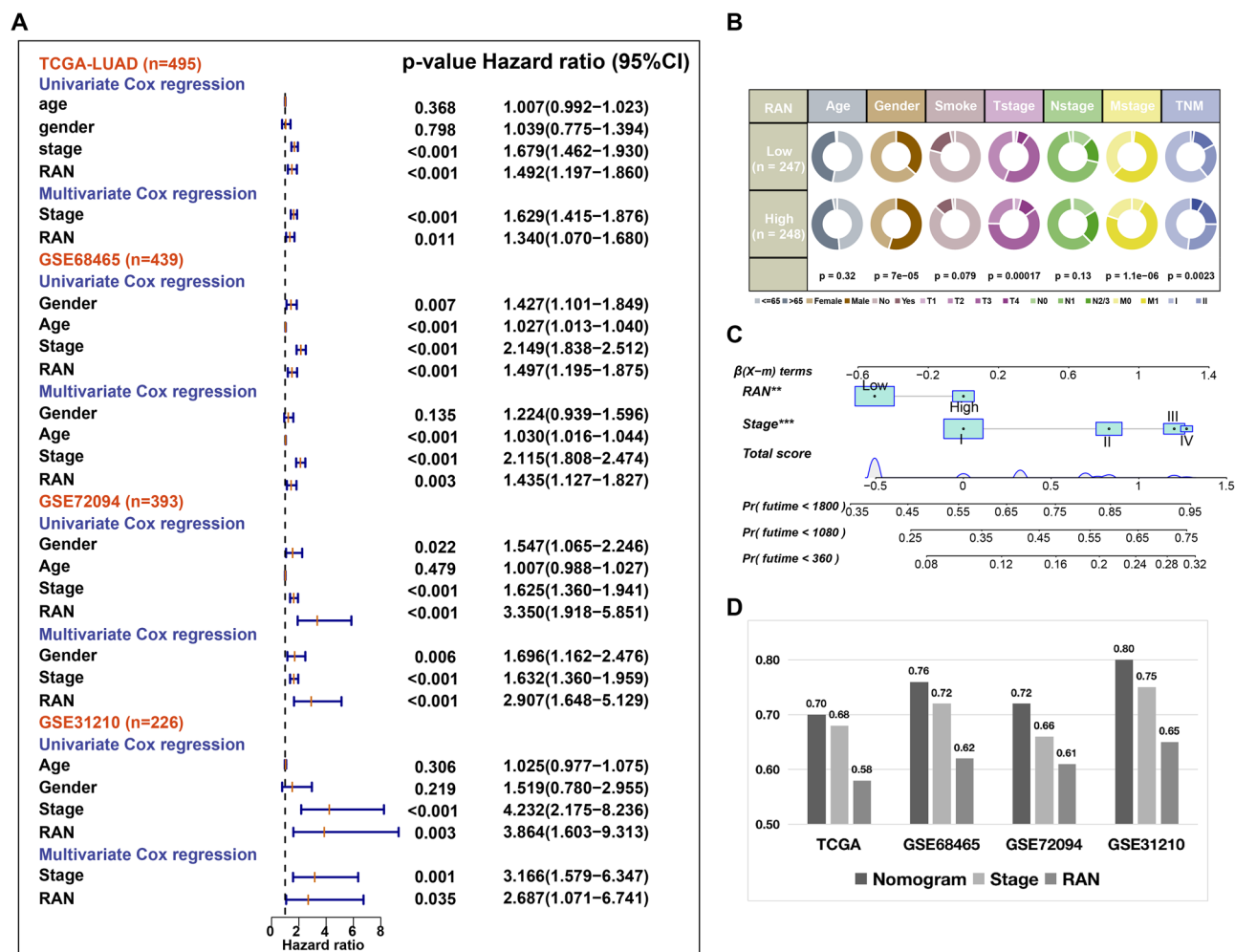
Fig. 2 | Prognostic analysis of RAN. A Forest plots exhibit the hazard ratio (HR), 95% confidence interval (CI), and corresponding P values derived from both univariate and multivariate Cox regression analyses across four LUAD cohorts. **B** A Circos plot illustrates the distribution of various clinical features in groups with high and low RAN expression. **C** An individualized prediction nomogram for overall survival (OS) has been constructed. **D** The predictive capabilities of the nomogram, TNM stage, and RAN expression for OS were assessed using the area under the receiver operating characteristic curve (AUC) for 3-year OS.

exhibited strong glycogen and vitamin B5 metabolism tumors showed strong glycogen and vitamin B5 metabolism, supporting rapid energy production for tumor growth and invasion[14]. The MPR group showed a distinct enrichment in amino acid metabolism pathways (glycine degradation, selenoamino acid metabolism, and glutamate pheromone receptor activity), while the NMPR group was characterized by increased lipid metabolism activity (sphingolipid, triglyceride, and fatty acid metabolism). Subsequently, we undertook a more in-depth exploration of the lipid metabolism levels in immune cells within NMPR tumor tissues (Fig. 1E, F). Our observations revealed that innate immune cells, like NK cells and fibroblasts, showed heightened lipid metabolism. In contrast, adaptive immune cells, specifically T and B cells, exhibited low lipid metabolism levels. Notably, among the crucial tumor-fighting immune T cells, those in the NMPR group had significantly lower lipid metabolism compared to T cells in both the MPR and control groups (Fig. 1F). As a result, we inferred that within the tumors of NMPR patients, tumor cells, fibroblasts, vascular endothelial cells, and other cell types displayed highly active lipid metabolism. This metabolic activity provided energy for tumor proliferation and migration, while simultaneously suppressing lipid metabolism in T cells under competitive conditions. This suppression facilitated tumor immune evasion and led to a reduced response to immunotherapy. Taken together, these findings highlight the metabolic traits of tumors pre- and post-immunotherapy, emphasizing lipid metabolism's role in therapy resistance.

RAN independently affects the prognosis of LUAD patients

We performed differentially expressed gene (DEG) analysis on residual tumor cells in the MPR and NMPR groups to identify key genes influencing the immune response. Using the criteria $|\log_2 (\text{fold change})|$ ($|\log_2 \text{FC}|$) > 0.5 and $p < 0.05$, we identified 725 genes with significant differential expression (Fig. 1G and Supplementary Fig. S1D, E). By intersecting these with 591 lipid metabolism-related genes, we found 23 common genes (Supplementary Fig. S1G). Among these, four were significantly linked to overall survival (OS) in LUAD patients from the TCGA database (Supplementary Fig. S1F). Notably, RAN was the only gene highly expressed in tumor cells compared to adjacent normal lung tissues (Fig. 1H and Supplementary Fig. S1H–J). Thus, we selected RAN as the candidate gene for this study.

We used Cox regression analysis to analyse the relationship between RAN expression levels and clinical characteristics of patients with LUAD, finding RAN to be an independent risk factor for OS in multiple LUAD databases: TCGA (HR = 1.340, 95% CI: 1.070–1.680), GSE68465 (HR = 1.435, 95% CI: 1.127–1.827), GSE72094 (HR = 2.907, 95% CI: 1.648–5.129), and GSE31210 (HR = 2.687, 95% CI: 1.071–6.741), all with p-values < 0.05 (Fig. 2A). Furthermore, within the TCGA database, elevated RAN expression was more prevalent in males and patients with advanced T, M, and TNM stages (Fig. 2B). By combining RAN expression with TNM stage, we developed a nomogram to predict 1-, 3-, and 5-year OS in LUAD patients
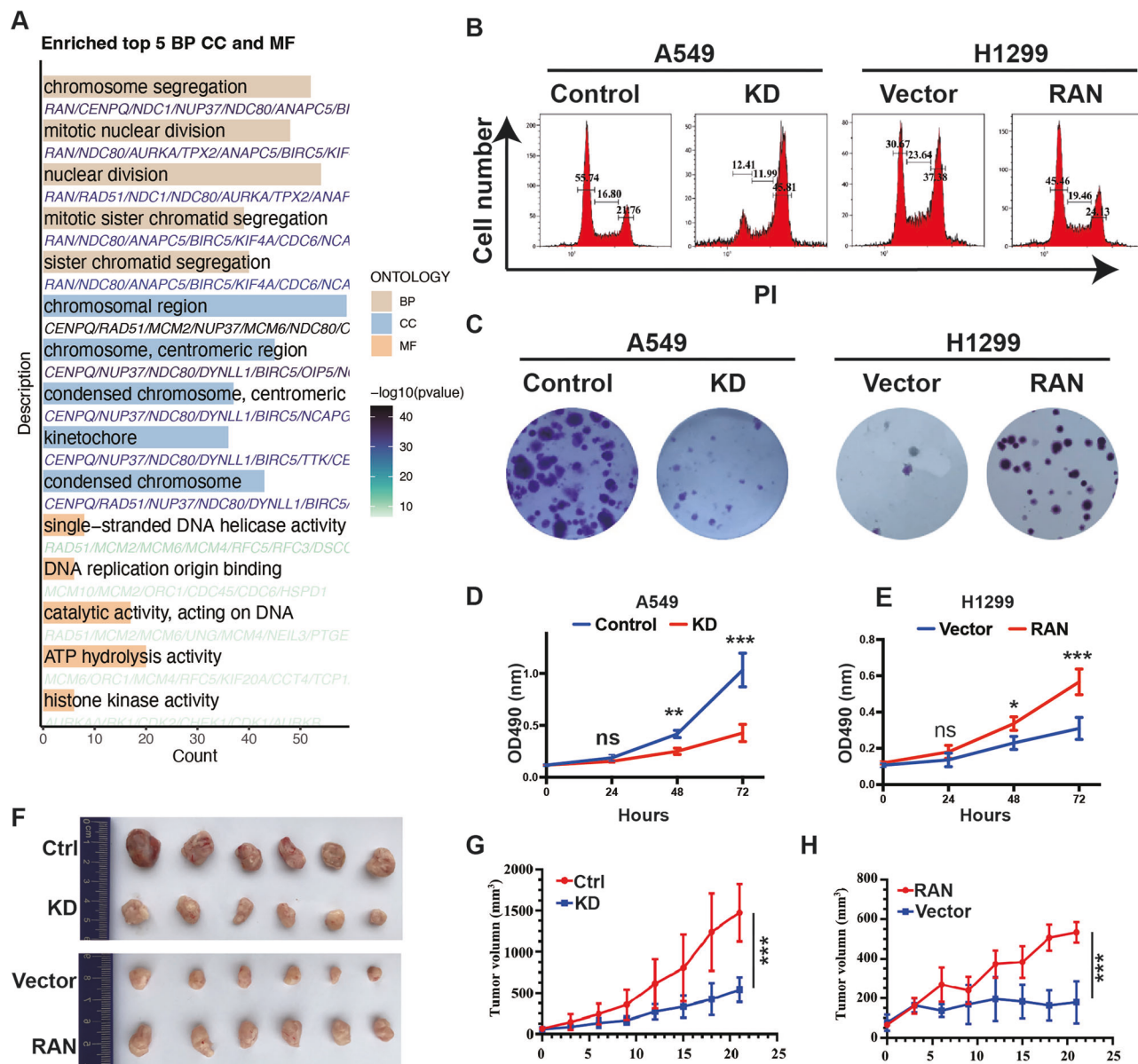
Fig. 3 | RAN promotes LUAD cell proliferation by regulating the cell cycle.
A Gene Ontology (GO) analysis of RAN in the TCGA database. **B** Cell cycle distribution of A549 and H1299 cells with silenced or overexpressed RAN. **C–E** Clone-forming ability (**C**) and proliferation capacity (**D, E**) of cells with RAN knockdown or overexpression, with cell viability confirmed using the CCK-8 assay. **F–H** Tumor collection (**F**) and growth curve of xenografts transfected with RAN-sg (**G**) or RAN plasmids (**H**). (Ns no significant; *$p < 0.05$; **$p < 0.01$; ***$p < 0.001$).

(Fig. 2C). This nomogram demonstrated superior predictive performance compared to TNM stage and RAN expression alone (Fig. 2D).

RAN promotes LUAD cell proliferation by regulating G2/M phase
We also identified 279 RAN-associated genes in the TCGA database for functional enrichment analysis using criteria of |Cor| > 0.6 and p < 0.05. The GO analysis shows that RAN mainly aids chromosome segregation during mitosis and can bind to DNA replication origins to promote replication, consistent with past research (Fig. 3A)[15,16]. In A549 and H1299 cell lines, RAN knockdown increased cells in the G2/M phase (21.76% to 45.81%), while RAN induction decreased this proportion (37.38% to 24.13%) (Fig. 3B, Supplementary Fig. S2A, B). Functional tests indicated that RAN knockdown significantly reduced the clonogenic ability and proliferation of A549 cells, while restoring RAN expression in H1299 cells reversed this effect (Fig. 3C–E). However, wound healing and Transwell assays showed that RAN expression did not affect the migratory or invasive

abilities of either cell line (Supplementary Fig. S2C, D). Additionally, xenograft tumor experiments revealed that tumors with RAN knockdown were smaller than those in the control group (Fig. 3F, G), whereas tumors with overexpression of RAN displayed accelerated progression.

RAN regulates metabolism by modulating the nucleoplasm localization of p-AMPK
We investigated how RAN, a gene tied to lipid metabolism, regulates LUAD metabolism using the IOBR database. RAN influences glucose, lipid, nucleotide, and amino acid metabolism, promoting purine and glycogen synthesis, fatty acid elongation, and methionine cycling, while inhibiting glycerophospholipid metabolism, linoleic acid metabolism and glycan degradation (Fig. 4A and Supplementary Fig. S3A–C). These metabolic perturbations are essential for maintaining the heightened proliferation and division rates of tumor cells, in addition to facilitating their evasion of immunosurveillance[17,18].
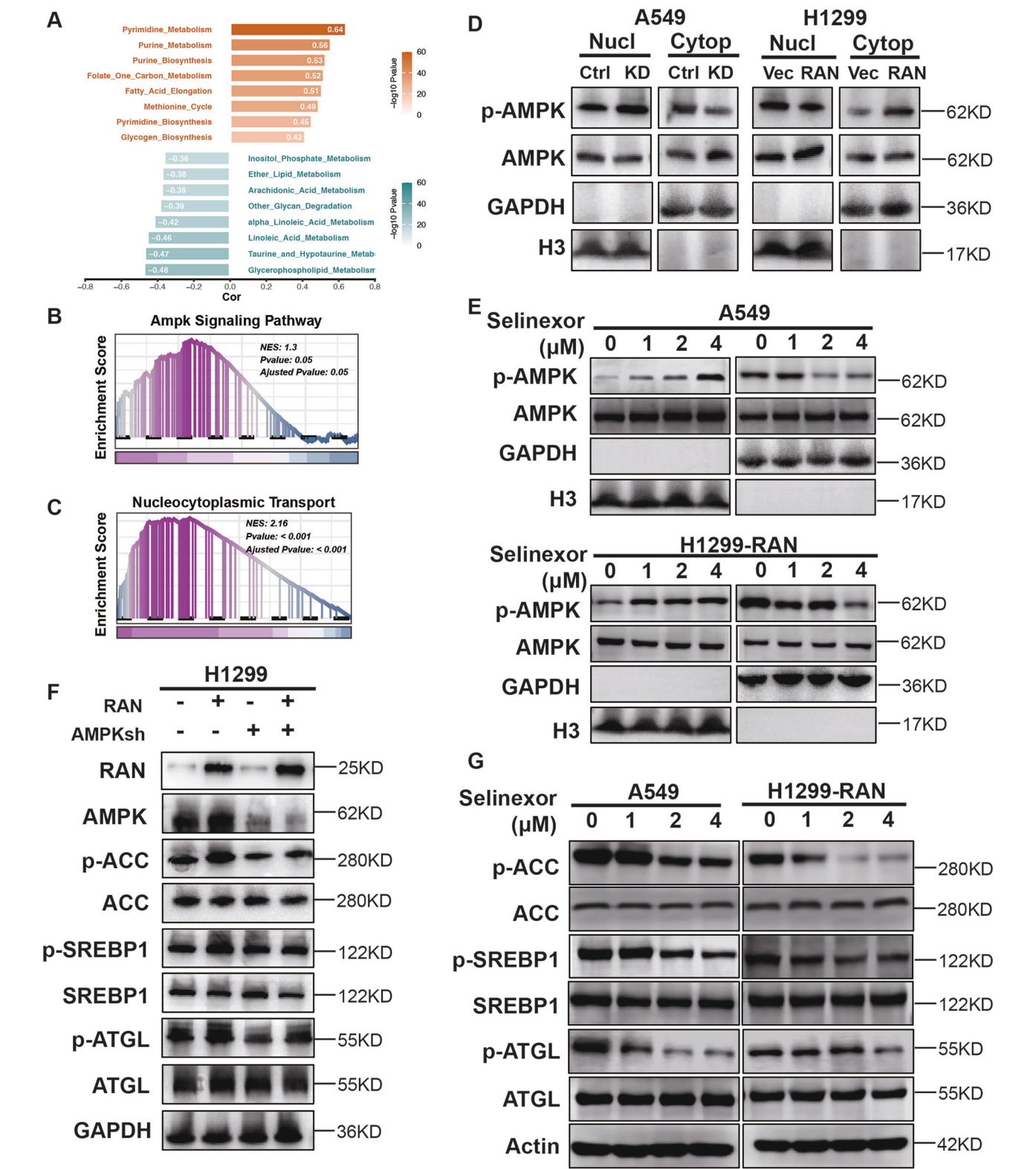
Fig. 4 | RAN reshapes the metabolic landscape of LUAD through Nuclear Export of p-AMPK. A Correlation analysis between RAN expression and the enrichment score of metabolic pathways in the TCGA database. **B** GSEA analysis demonstrating the correlation between RAN expression and AMPK Pathway gene sets in the TCGA database. **C** GSEA analysis showing the correlation between RAN expression and Nucleocytoplasmic Transport Pathway gene sets in the TCGA database. **D** Western blotting reveals the distribution of AMPK after RAN knockdown or overexpression. **E** Western blotting detects the distribution of AMPK in the cytoplasm and nucleus following Selinexor treatment in A549 and H1299-RAN cell. **F** Western blot analysis reveals the expression levels of AMPK downstream target genes following RAN overexpression, both in the presence and absence of AMPK knockdown. **G** Western blot displays the expression of AMPK downstream target genes after Selinexor treatment. GAPDH and histone H3 were used to confirm equal protein loading and the purity of cytoplasmic and nuclear fractions, respectively.

The AMPK pathway, a key energy sensor, manages glucose, lipid, and protein homeostasis under stress. GSEA analysis shows that RAN expression activates the AMPK and nucleocytoplasmic transport pathways (Fig. 4B, C, Supplementary Fig. S3D). Previous studies have identified nuclear export sequences in the AMPK gene, enabling its movement from the nucleus to the cytoplasm through the XPO1-RAN-GTP complex[19,20]. Therefore, we investigated whether knockdown or overexpression of RAN could alter the localization of AMPK in the cytoplasm and nucleus. Our findings indicated that RAN expression had no significant effect on the protein levels of AMPK or p-AMPK in whole-cell lysates (Supplementary Fig. S4A). However, knocking down RAN resulted in increased nuclear accumulation of p-AMPK (Fig. 4D). In contrast, overexpressing RAN promoted p-AMPK distribution in the cytoplasm. We treated wild-type A549 and 1299-RAN cells, as well as Lewis LUAD cells, with the nuclear export inhibitor Selinexor, which specifically targets the XPO1-RAN-GTP complex. We then observed a gradient-dependent aggregation of p-AMPK expression in the nuclear of the cells after Selinexor treatment (Fig. 4E and Supplementary Fig. S4B). Overexpression of RAN also enhanced the phosphorylation of AMPK downstream targets, including Acetyl-CoA Carboxylase (ACC), Sterol regulatory element–binding protein 1 (SREBP1), and adipose triglyceride lipase (ATGL) in H1299 cell. However, this effect was hindered by the knockdown of AMPK (Fig. 4F). Furthermore, Selinexor suppressed the phosphorylation of ACC, SREBP1, and ATGL in a dose-dependent manner in A549 and RAN-overexpressed H1299 cells (Fig. 4G).

RAN impairs LUAD cell antigen presentation to promote immune tolerance

Solid tumor tissue consists mainly of tumor, stromal, and immune cells[21]. Patients with high RAN expression showed increased tumor purity and reduced stromal and Estimate scores compared to those with low RAN expression (all $p < 0.01$) (Fig. 5A, B). Additionally, the ssGSEA algorithm found a negative correlation between RAN expression and the infiltration of several antitumor immune cells, such as dendritic cells, activated B cells, monocytes, mast cells, natural killer cells, and effector memeory CD8 T cells, as well as Type1 T helper cells (all $p < 0.01$) (Fig. 5C). A positive correlation was found with Memory B cells, CD4 + T cells, and Type2 T helper cells (all $p < 0.01$). RAN showed no correlation with immune checkpoints like CTLA-4, LAG3, and PDCD1 (Fig. 5D). However, high RAN expression was linked to low expression of immune stimulators (e.g., CD27, CD28, CXCL12) and MHC molecules (e.g., HLA-A, HLA-B, HLA-C). These findings suggest that tumors with high RAN expression have increased invasiveness and a more suppressed immune microenvironment.

IPS is a reliable machine learning algorithm for assessing tumor response to immunotherapy[22]. RAN negatively correlates with IPS and MHC scores in the TCGA and GSE60052 databases, suggesting that higher RAN expression indicates lower immunogenicity and antigen presentation (Fig. 5E, F). Using the tumor immune dysfunction and exclusion (TIDE) algorithm, patients with high RAN expression had significantly higher TIDE scores, indicating a greater potential for immune evasion, compared to those with low RAN expression (all $p < 0.001$) (Fig. 5G, I). The high RAN expression group had a significantly lower proportion of estimated immune responders compared to the low RAN expression group in both the TCGA and GSE60052 databases ($p < 0.001$) (Fig. 5H, J). To further substantiate the predictive value of RAN expression in clinical settings, we examined several immunotherapy cohorts. In the GSE126044 cohort, none of the 8 patients with high RAN expression responded to Nivolumab, while 5 of 8 patients with low RAN expression experienced complete or partial remission (AUC = 0.857) (Fig. 5K, L). In a cohort of NSCLC patients on anti-PD1 therapy, low RAN expression predicted responders with 61.5% (8/13) sensitivity and 90.7% (39/43) specificity (Fig. 5M, N).

In the GSE207422 database, MPR patient tumors showed increased HLA-A, B, C, DR, and DP expression and higher MHC-I antigen presentation scores compared to NMPR patients (Fig. 6A, B, D). Previous research connecting MHC-I to CD8 T-cell activation prompted us to isolate and repopulate tumor T cells, identifying CD8+ populations using CD8A

and CD8B markers (Supplementary Fig. S5A–D)[23,24]. Notably, the NMPR group exhibited a significantly higher exhaustion signature in CD8 + T cells than the MPR group (Fig. 6C, E). We propose that the poor immunotherapy response in NMPR patients may be due to low CD8 + T-cell activation from reduced tumor immunogenicity. In A549 cells, the knockdown of RAN led to an increase in the expression of HLA-ABC and DR. However, this effect was reversed when AMPK was inhibited (Fig. 6F). Furthermore, Selinexor treatment elevated HLA-ABC and DR levels in LUAD cells in a dose-dependent manner (Fig. 6G). Nevertheless, subsequent AMPK knockdown abolished the enhanced expression of HLA-ABC and DR induced by Selinexor (Fig. 6G). These findings suggest that targeted inhibition of the nuclear export of p-AMPK can suppress the expression of MHC molecules in tumor cells, thereby diminishing their immunogenicity and impeding the activation of immune cells within the TME.

## Selinexor potentiates the efficacy of Anti-PD-1 therapy in Xenograft mice

These findings prompted us to investigate if disrupting RAN's nuclear export could improve anti-PD-1 therapy by altering the metabolic and immune environments in LUAD. We created a xenograft mouse model with Lewis LUAD cells and, on day 7 after tumor implantation, treated the mice with anti-PD-1 antibody, Selinexor, or both (Fig. 7A). The combined therapy significantly inhibited tumor growth more than control and monotherapy, with acceptable effects on mouse body weight and organ toxicity (Fig. 7B–E). Previous studies have highlighted the crucial role of MHC-I molecule expression on the surface of tumor cells in enabling CD8 + T cells to recognize tumor antigens and trigger immunological responses[24]. Flow cytometry showed no significant difference in CD8 T-cell infiltration among subgroups, but the combination therapy increased the infiltration of IFN-γ + CD8 T-cells (Fig. 7F, G, Supplementary Fig. S6). We also retrospectively gathered clinical data and biopsy samples from elderly patients with advanced LUAD undergoing ICB monotherapy (Fig. 7H). Subsequently, we investigated the potential of immunohistochemistry (IHC) detection of RAN as a predictive marker for immunotherapy response in LUAD (Fig. 7I). As expected, the IHC score for RAN was significantly elevated in LUAD patients who responded to anti–PD-1 therapy compared to nonresponders (mean scores: 39.8 vs. 152.8, $p = 0.005$) (Fig. 7J).

Discussion

Numerous studies highlight RAN's crucial roles in biological processes like chromosome segregation, nuclear export, autophagy suppression, and ferroptosis[15,25–27]. However, its role in anti-tumor immune responses is under-researched. Our study employed bioinformatics and experiments to explore RAN's functions, revealing a strong link to tumor therapy response. We discovered that RAN may promote immune tolerance through lipid metabolism reprogramming via nuclear export of p-AMPK and reduced MHC molecule expression on tumor cells, which hinders immune cell activation. Thus, combining nuclear export inhibitors with immunotherapy might effectively counter immune tolerance and boost anti-tumor responses. Our research offers new insights into RAN's role in anti-tumor immunity and suggests potential therapeutic strategies for further study.

Tumor cells adapt metabolically to various signals, triggering transformation or growth[13]. During rapid tumour cell proliferation, fatty acids are crucial for membrane biosynthesis and serve as a significant energy source under stressful conditions[28]. Huang et al. found that tumor cells' fatty acid uptake and oxidation deplete these nutrients in the TME, hindering CD8 + T cell activation and lowering IFN-γ secretion[29]. In pancreatic ductal adenocarcinoma, phosphatidylinositol accumulation in the TME impairs CD8 + T cell mitochondria, causing lipotoxicity[30]. Chen et al. found that MK1775 improved anti-PD-1 therapy by modifying fatty acid interactions with tumor-associated macrophages and CD8 + T cells[10]. Our re-analysis of scRNA-seq data revealed that glucose metabolism is crucial for meeting the energy needs of normal tumor cells. After the administration of immunotherapy, the tumors demonstrated two distinct metabolic profiles: NMPR
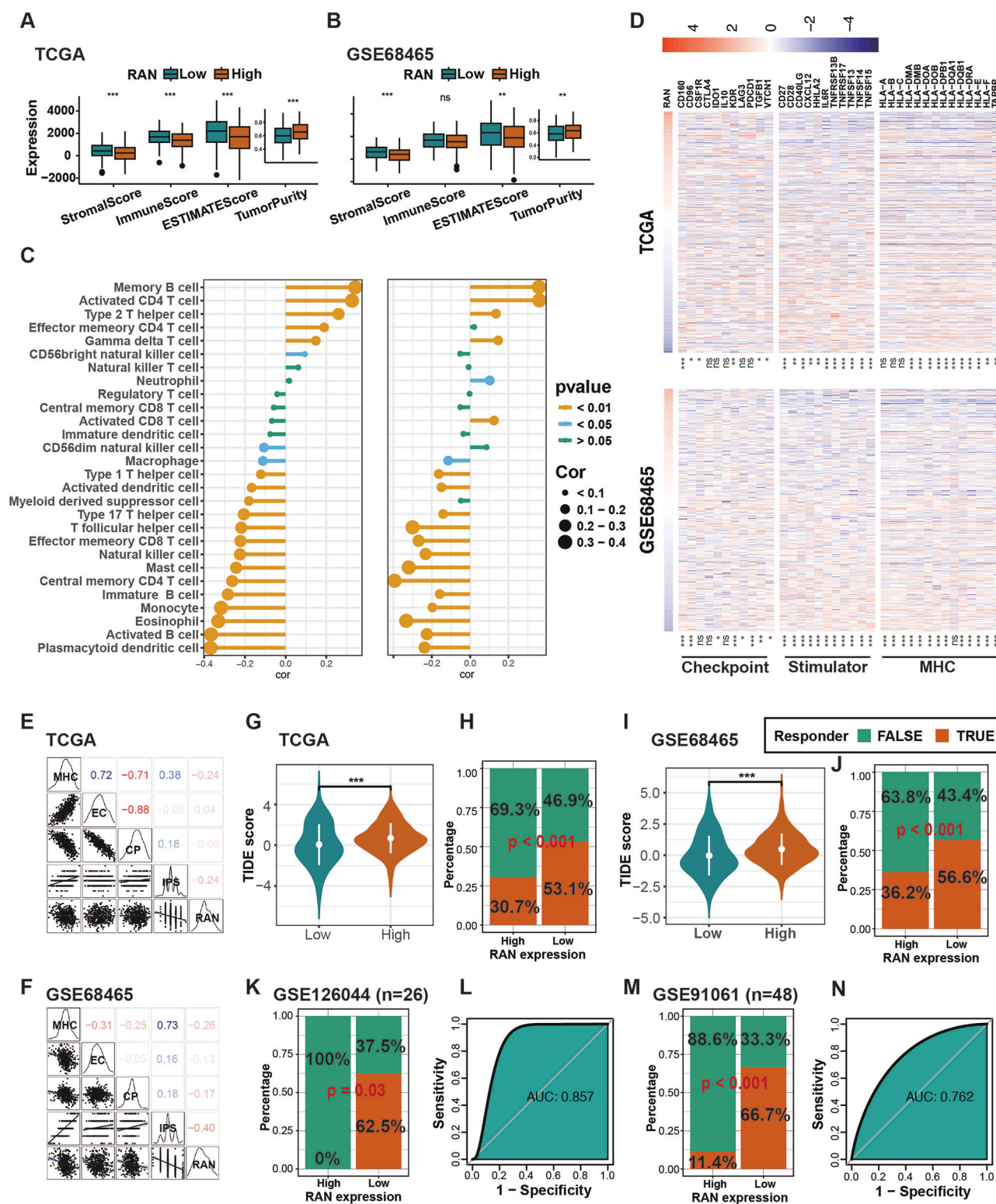
Fig. 5 | RAN expression Indicates poor response to immunotherapy in LUAD. A, B Comparisons of the ESTIMATE score, immune score, stromal score, and tumor purity between groups with low and high RAN expression in the TCGA cohort (**A**) and GSE68465 database (**B**). **C** Correlation analysis between the levels of 28 immune cells and RAN expression. **D** Pearson correlation coefficients between RAN and representative immune genes. **E, F** Correlations between RAN and MHC molecules (MHC), effector cells (EC), immunomodulators (CP), suppressor cells (SC), and immunophenoscore (IPS) in the TCGA database (**E**) and GSE68465 (**F**).

G, I Comparison of the tumor immune dysfunction and exclusion (TIDE) scores between the high and low RAN expression groups in the TCGA database (**G**) and GSE69465 (**I**). The proportions of responders and non-responders in the low and high RAN expression groups in the TCGA (**H**), GSE68465 (**J**), GSE126044 (**K**), and GSE91061 (**M**) datasets. **L, N** Receiver Operating Characteristic (ROC) curves of RAN expression for predicting patient response to immunotherapy. ns not significant; *$p < 0.05$; **$p < 0.01$; ***$p < 0.001$.
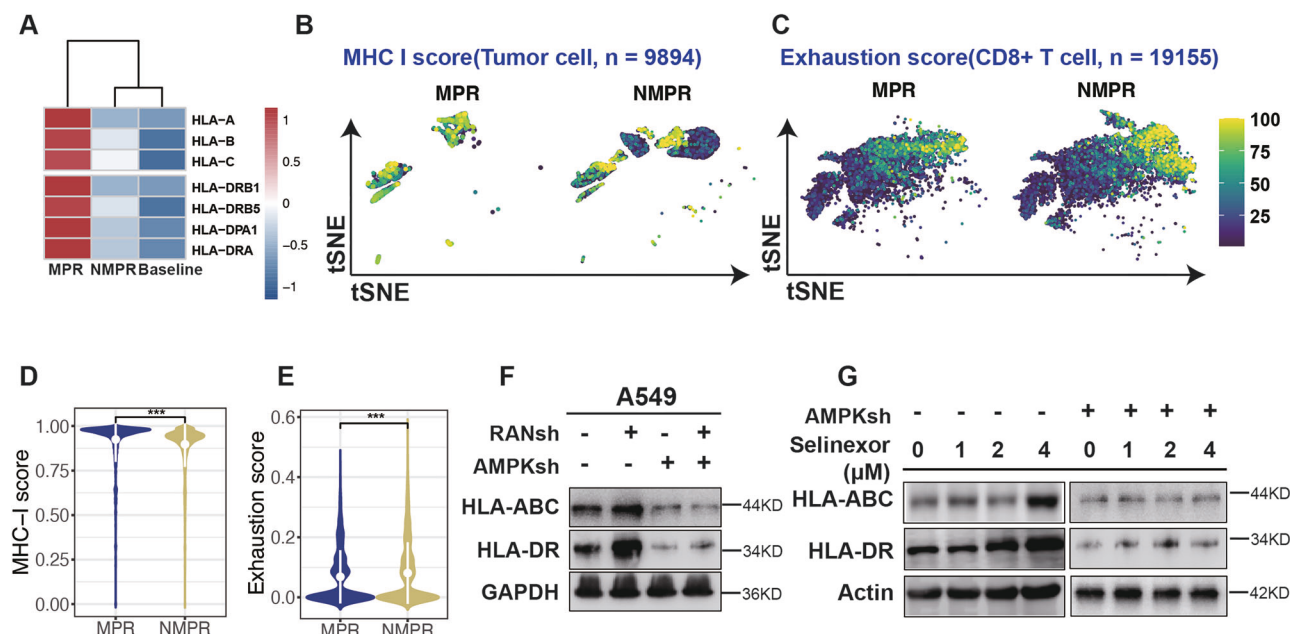
Fig. 6 | RAN downregulates immunogenicity of LUAD. A A heatmap illustrates the relative expression of MHC molecules in tumor cells among the baseline, MPR, and NMPR groups. B, C Distribution of the MHC-I score (B) and CD8 T cell exhaustion score (C) between the MPR and NMPR groups. D, E Differences in the MHC-I score (D) and CD8 T cell exhaustion score (E) between the MPR and NMPR groups. F Western blotting shows the expression of HLA-ABC and HLA-DR after RAN knockdown or overexpression. G Western blotting demonstrates the expression of HLA-ABC and HLA-DR after Selinexor treatment. ***$p < 0.001$.

tumors were predominantly characterized by lipid metabolism, including fatty acids, glycosphingolipids, sphingolipids, and triglyceride, whereas MPR tumors primarily exhibited amino acid metabolism, particularly involving selenoamino acids and glutamate. We propose that the increased activity of specific lipid metabolic pathways in NMPR tumors may represent a potential mechanism by which tumor cells evade the immune system.

RAN is integral to the malignant progression of tumor cells across various cancers, such as ovarian cancer, hepatocellular carcinoma, and gastric cancer[27,31,32]. Prior studies have demonstrated that the inhibition of RAN-dependent nucleoplasmic transport processes can effectively suppress proliferation by disrupting cell cycle progression in pancreatic ductal carcinoma[33]. Wang K and his team discovered that knocking down RAN significantly reduces the stemness of triple-negative breast cancer, indicating a promising approach for targeted therapy in tumors characterized by high stemness[34,35]. Furthermore, Galiger C et al. have demonstrated that the inhibition of RAN can reduce the adaptability of energy metabolism in neuroblastoma by suppressing oxidative phosphorylation[36]. In our study, we identified RAN as a poor prognostic indicator in LUAD across several independent databases. In vivo experiments further substantiated that RAN knockdown induced arrest in the M2 phase in LUAD cells, significantly reducing cell proliferation, clone formation, and tumor progression.

TME play a crucial role in tumor progression[37]. Various studies have highlighted RAN as a key gene regulating innate immune phagocytosis in response to viral infections[38,39]. Qiao et al. discovered that RAN is essential for T-cell activation, potentially by enhancing nuclear retention of the critical transcription factor c-Jun[40]. Prior research revealed a significant correlation between RAN expression and CD4 + T-cell infiltration across multiple cancers. RAN promotes CD4 + TH2 cell differentiation by boosting IL-4 secretion from tumor cells, suggesting a potential target for modulating the tumor immune microenvironment in oral squamous cell carcinoma[41]. In our study, we similarly observed a positive correlation between RAN expression and TH2 cells. Furthermore, we found that RAN can decrease the immunogenicity of tumor cells by inhibiting the expression of MHC-related molecules, enabling them to evade immune recognition and resulting in a low infiltration of various anti-immune cells within the TME, which unveils a previously unrecognized mechanism of RAN in tumor immunomodulation. Future research could focus more intensively on unraveling the role of the immune microenvironment in boosting the effectiveness of Selinexor-sensitized immunotherapy, including pinpointing the key immune cell populations responsible for executing the primary functions and elucidating the underlying mechanisms at work.

RAN interacts with transporter proteins to control nucleoplasmic transport. The main approach to stopping nucleoplasmic shuttling for tumor eradication is targeting these proteins[42]. Selinexor, an FDA-approved nuclear export inhibitor since 2019 for relapsed multiple myeloma, has been tested in various preclinical and Phase II/III trials[43–45]. The NCT03555422 study showed that oral Selinexor notably enhanced progression-free survival (PFS) in 263 endometrial cancer patients, particularly those with TP53 wild-type tumors, compared to placebo[45]. Similarly, the GEM-SELIBORDARA study found that adding Selinexor to standard treatment extended PFS in multiple myeloma patients to 24 months, compared to 7 months without it[44]. Selinexor is being studied for its ability to enhance first-line chemotherapy, improve the tumor immune environment, and work synergistically with immunotherapy[46–48]. Altan M, et al. found that combining Selinexor with pembrolizumab showed promising antitumor activity in metastatic NSCLC patients without overlapping toxicities[49]. Our study revealed that the targeted inhibition of nuclear export significantly enhanced CD8 + T-cell activity. Moreover, the combined therapeutic regimen of Selinexor and anti-PD1 demonstrated a robust inhibitory effect in Xenograft mouse. These findings offer theoretical support for the development of future combined therapeutic strategies for NSCLC.

It is essential to recognize certain limitations inherent in this study. Our analyses are primarily based on bioinformatics assessments of publicly available sequencing data, which require additional in vivo and in vitro validation to accurately determine the true TME of LUAD. Single-cell metabolomics offers a promising approach for exploring cellular heterogeneity and understanding the functional status of individual cells[50]. Given that Selinexor is not a selective inhibitor of RAN nuclear export, our current study merely suggests that the synergistic effect of Selinexor in combination with anti-PD-1 therapy might be RAN-dependent. However, whether targeted inhibition of RAN can enhance the efficacy of anti-PD-1 therapy remains to be further elucidated in future research. Furthermore, the cellular gene regulatory network is complex, multifaceted, and
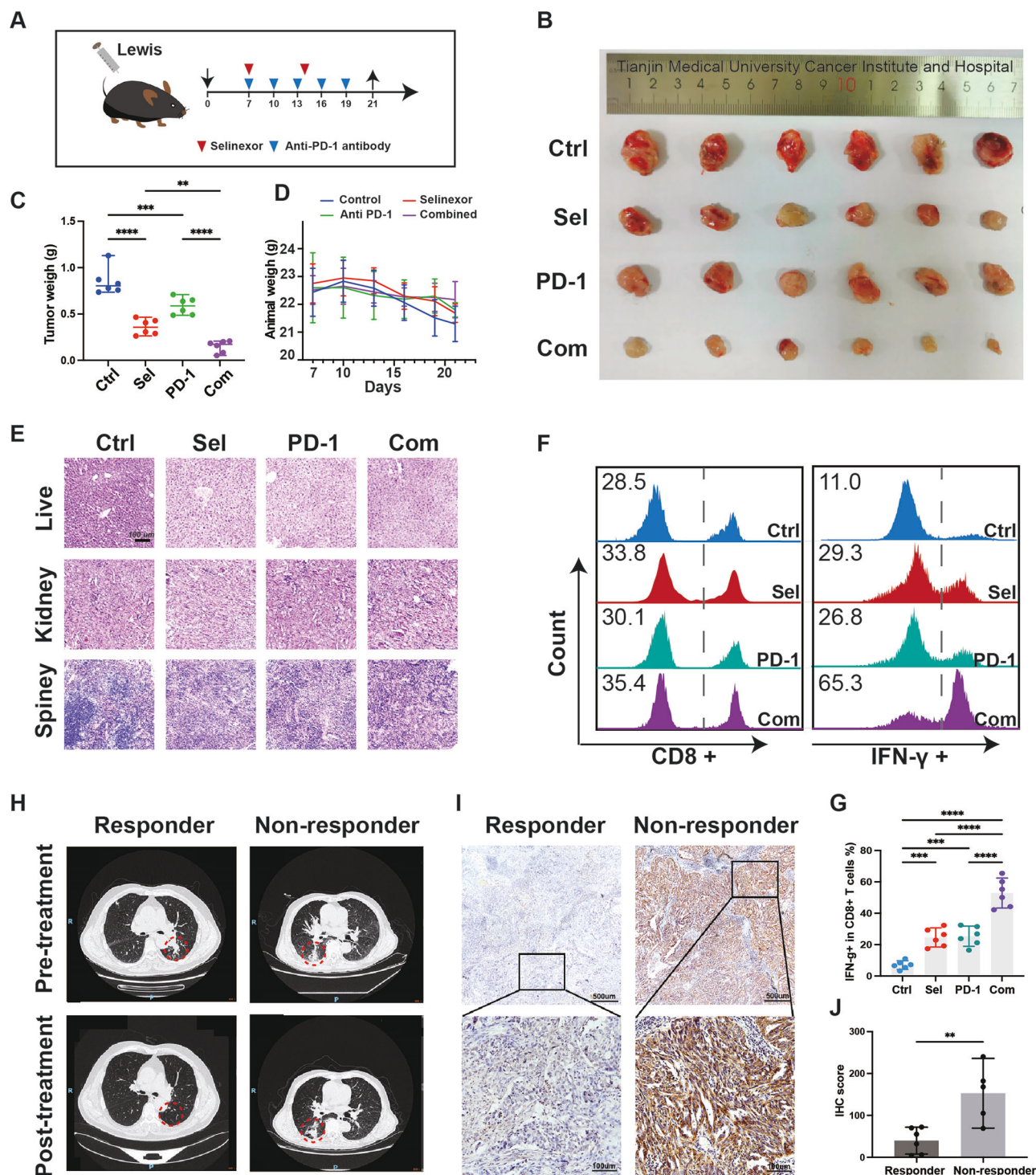
Fig. 7 | Blockage of nuclear export signaling potentiates the efficacy of Anti–PD-1 therapy. A Schematic representation of the treatment schedule for anti–PD-1 therapy and the nuclear export antagonist Selinexor in xenograft mice. **B** Gross appearance of orthotopic LUAD tumors from the indicated treatment groups. **C, D** Tumor weight (**C**) and tumor volume (**D**) of each group at the endpoint. **E** H&E staining was used to observe the side effects of Selinexor and the PD-1 monoclonal antibody. **F** Representative flow cytometry dot plots and proportions of CD8 + T cells and IFN-γ + CD8 T cells in tumors from treated C57BL/6 mice.

G The proportions of IFN-γ+ cells within CD8 + T cells in the indicated groups are shown ($n = 6$ mice per group). **H** Representative cross-sectional images of chest computed tomography before and after treatment in patients with and without a response to ICIs. **I** Representative immunohistochemical staining images of RAN in LUAD tissues from patients with and without a response to ICIs. **J** Comparison of IHC scores of RAN in patients with and without a response to ICIs. **$*p < 0.01$; ***$p < 0.001$; ****$p < 0.0001$.

dynamic. The precise mechanisms underlying how RAN influences tumor cell immunogenicity and immune tolerance necessitate further exhaustive exploration.

In summary, lipid metabolic remodeling is a critical feature of tumors in response to immunotherapy. Our study identifies RAN as a novel potential target for predicting the efficacy of immunotherapy and provides

new perspectives and valuable insights for the development of future combination therapy strategies for LUAD.

Methods

Data collection and preprocessing

ScRNA-seq data for 15 NSCLC specimens, pre- and post-PD-1 blockade, were obtained from GSE207422. Additionally, four bulk RNA-seq datasets for LUAD patients (n = 1553) were sourced from The Cancer Genome Atlas (TCGA; https://portal.gdc.cancer.gov) and the Gene Expression Omnibus (GEO; https://www.ncbi.nlm.nih.gov/geo/). The transcripts per kilobase of exon model per million mapped reads (TPM) expression profile was normalized using $\log2(x + 1)$ transformation as needed. RNA-seq data and clinical details for tumors treated with immunotherapy were sourced from GSE126044 and GSE91061. This included 26 NSCLC patients from GSE126044 sampled before anti-PD-1 therapy and 48 melanoma patients from GSE91061 sampled during anti-CTLA4 and anti-PD1 treatment. Between January 2020 and January 2021, clinical data and biopsy samples were collected from elderly patients with advanced LUAD who underwent monotherapy with ICB at the Tianjin Medical University Cancer Institute and Hospital. This study was approved by the ethics committee of the Tianjin Medical University Cancer Institute and Hospital (Ek2021098). The informed consent was waived by the ethics committee of the Tianjin Medical University Cancer Institute and Hospital.

ScRNA-seq analysis

Single-cell data were analyzed with the 'Seurat' package under previously established condition[51]. Cell clustering was performed using the 'tSNE' algorithm, and DEGs in different clusters were identified with the 'FindAllMarkers' function. Broad cell types were determined by marker gene expression[51,52]. Metabolism-related pathway enrichment scores were calculated using the 'scMetabolism' package and the Reactome database, which includes 82 metabolic pathways[53].

Bulk RNA-seq analysis

Gene sets of "metabolism of lipids" was obtained from Reactome database (https://reactome.org/download-data/). DEGs between tumor and adjacent normal tissues were identified using the 'limma' package with criteria of $|\log2\ FC| > 0.5$ and p-value < 0.05. Genes linked to RAN were found using Pearson's correlation ($|Cor| > 0.6$, p-value < 0.05) and analyzed for functional enrichment via 'clusterProfiler'. The metabolism score for each LUAD sample was calculated using the 'ssgsea' algorithm in the 'IOBR' package, based on 102 published tumor metabolism gene signatures.

The "ESTIMATE" algorithm calculated scores for tumor purity, immune, and stromal components for each patient, while "CIBERSORT" evaluated immune cell infiltration. Immunophenotype (IPS) scores, predicting response to anti-PD1 and anti-CTLA4 therapies, were determined using the 'IOBR' package[54]. The TIDE score, from the TIDE database, assessed the potential for tumor immune escape[55].

Cell culture and transfection

Human and mouse LUAD cell lines A549, H1299, and Lewis were sourced from the American Type Culture Collection and grown in RPMI 1640 and DMEM media with 10% fetal bovine serum. Lentiviral vectors for human RAN sgRNA and full-length RAN were obtained from the Public Protein/Plasmid Library. HEK293T cells were transfected with these lentiviral and packaging plasmids to produce lentivirus. Lentivirus was produced by transfecting HEK293T cells with the lentiviral and packaging plasmids. Stable cell lines were created by treating the cells' supernatant for 48 h and selecting with 2 µg/mL puromycin.

IHC Staining, Western Blotting (WB), Nuclear and cytoplasmic fractions, Flow Cytometry, and Phenotypic Assays

IHC staining, WB assays, Flow Cytometry staining, and functional tests like CCK8, wound healing, and Transwell matrix assays were performed as previously described[56,57]. Primers and antibodies are detailed in Supplementary Table S1. Two pathologists independently evaluated IHC results using a semiquantitative method, categorizing staining intensity as negative (0), weak (0-1), moderate (1-2), or strong (2-3)[58]. Nuclear and cytoplasmic fractions were extracted using NE-PER Nuclear and Cytoplasmic Extraction Reagents (#78833, Thermo Scientific) according to the manufacturer's protocol.

Xenograft experiments

1×10^6 LUAD cells in 100 uL PBS were injected subcutaneously into 6-week-old female C57 mice. After one week, mice were divided into groups of six and treated with either a vehicle control, anti-PD1 antibody (10 mg/kg, ip, twice weekly), Selinexor (5 mg/kg, p.o., once weekly), or both. Tumor growth was measured every two days by recording the longest (a) and shortest (b) tumor diameters. Tumor volume (V, mm³) was determined with the formula $V = a \times b^2/2$. Mice were euthanized via painless cervical dislocation once their tumors reached a volume of 1500 mm³. The study followed protocols approved by the Animal Care and Use Committee of Tianjin Cancer Institute & Hospital, Tianjin Medical University (NSFC-AE-2021122). All methods were performed in accordance with the relevant guidelines and regulations. This study is adhered to the ethical guidelines of the Helsinki Declaration.

Statistical analyses

Statistical analyses were performed with R (v4.2.2) and Prism (v9.5.0), considering p-values below 0.05 as significant. T-tests or Wilcox tests were used for continuous data, while chi-square or Fisher's tests were used for categorical data.

Data availability

The data sets used in this investigation are available through public repositories. The article contains the names of the repository/repositories.

Code availability

The code used for analysis can be accessed by the corresponding author on reasonable request.

References

1. Siegel, R. L. et al. Cancer statistics, 2023. *CA Cancer J. Clin.* **73**, 17–48 (2023).
2. Passaro, A. et al. Managing Resistance to Immune Checkpoint Inhibitors in Lung Cancer: Treatment and Novel Strategies. *J. Clin. Oncol.* **40**, 598–610 (2022).
3. Nimptsch, K. et al. Prospective and Mendelian randomization analyses on the association of circulating fatty acid binding protein 4 (FABP-4) and risk of colorectal cancer. *BMC Med.* **21**, 391 (2023).
4. Xu, D., Yin, S. & Shu, Y. NF2: An underestimated player in cancer metabolic reprogramming and tumor immunity. *NPJ Precis Oncol.* **8**, 133 (2024).
5. Martin-Perez, M. et al. The role of lipids in cancer progression and metastasis. *Cell Metab.* **34**, 1675–1699 (2022).
6. Pascual, G. et al. Targeting metastasis-initiating cells through the fatty acid receptor CD36. *Nature* **541**, 41–45 (2017).
7. Altuna-Coy, A. et al. The lipidomic profile of the tumoral periprostatic adipose tissue reveals alterations in tumor cell's metabolic crosstalk. *BMC Med.* **20**, 255 (2022).
8. Xu, S. et al. Uptake of oxidized lipids by the scavenger receptor CD36 promotes lipid peroxidation and dysfunction in CD8(+) T cells in tumors. *Immunity* **54**, 1561–1577.e7 (2021).
9. Poznanski, S. M. et al. Metabolic flexibility determines human NK cell functional fate in the tumor microenvironment. *Cell Metab.* **33**, 1205–1220.e5 (2021).

10. Chen, Y. et al. Harnessing lipid metabolism modulation for improved immunotherapy outcomes in lung adenocarcinoma. *J. Immunother. Cancer*;**12**, https://doi.org/10.1136/jitc-2024-008811 (2024).

11. Liu, L. et al. Targeting inhibition of prognosis-related lipid metabolism genes including CYP19A1 enhances immunotherapeutic response in colon cancer. *J. Exp. Clin. Cancer Res.* **42**, 85 (2023).

12. Kim, J. & DeBerardinis, R. J. Mechanisms and Implications of Metabolic Heterogeneity in Cancer. *Cell Metab.* **30**, 434–446 (2019).

13. Faubert B., Solmonson A., DeBerardinis R. J. Metabolic reprogramming and cancer progression. *Science* **368**, https://doi.org/10.1126/science.aaw5473 (2020).

14. Tufail, M., Jiang, C. H. & Li, N. Altered metabolism in cancer: insights into energy pathways and therapeutic targets. *Mol. Cancer* **23**, 203 (2024).

15. Kiyomitsu, A. et al. Ran-GTP assembles a specialized spindle structure for accurate chromosome segregation in medaka early embryos. *Nat. Commun.* **15**, 981 (2024).

16. El-Tanani, M. et al. Ran GTPase and Its Importance in Cellular Signaling and Malignant Phenotype. *Int. J. Mol. Sci.* **24**, https://doi.org/10.3390/ijms24043065 (2023).

17. Hung, M. H. et al. Tumor methionine metabolism drives T-cell exhaustion in hepatocellular carcinoma. *Nat. Commun.* **12**, 1455 (2021).

18. Sun, L., Zhang, H. & Gao, P. Metabolic reprogramming and epigenetic modifications on the path to cancer. *Protein Cell.* **13**, 877–919 (2022).

19. Fukuda, M. et al. CRM1 is responsible for intracellular transport mediated by the nuclear export signal. *Nature* **390**, 308–311 (1997).

20. Kazgan, N. et al. Identification of a nuclear export signal in the catalytic subunit of AMP-activated protein kinase. *Mol. Biol. Cell.* **21**, 3433–3442 (2010).

21. Yoshihara, K. et al. Inferring tumour purity and stromal and immune cell admixture from expression data. *Nat. Commun.* **4**, 2612 (2013).

22. Hugo, W. et al. Genomic and Transcriptomic Features of Response to Anti-PD-1 Therapy in Metastatic Melanoma. *Cell* **165**, 35–44 (2016).

23. Bischoff, P. et al. Single-cell RNA sequencing reveals distinct tumor microenvironmental patterns in lung adenocarcinoma. *Oncogene* **40**, 6748–6758 (2021).

24. Sharma, G. et al. A synthetic cytotoxic T cell platform for rapidly prototyping TCR function. *NPJ Precis Oncol.* **8**, 182 (2024).

25. Cao, L. et al. Inhibition of RAN attenuates influenza a virus replication and nucleoprotein nuclear export. *Emerg. Microbes Infect.* **13**, 2387910 (2024).

26. Liu, X. et al. RSL1D1 promotes the progression of colorectal cancer through RAN-mediated autophagy suppression. *Cell Death Dis.* **13**, 43 (2022).

27. Yuan, Y. et al. CLTRN, Regulated by NRF1/RAN/DLD Protein Complex, Enhances Radiation Sensitivity of Hepatocellular Carcinoma Cells Through Ferroptosis Pathway. *Int J. Radiat. Oncol. Biol. Phys.* **110**, 859–871 (2021).

28. Koundouros, N. & Poulogiannis, G. Reprogramming of fatty acid metabolism in cancer. *Br. J. Cancer* **122**, 4–22 (2020).

29. Huang, T. X. et al. ATP6V0A1-dependent cholesterol absorption in colorectal cancer cells triggers immunosuppressive signaling to inactivate memory CD8(+) T cells. *Nat. Commun.* **15**, 5680 (2024).

30. Wang, R. et al. Intratumoral lipid metabolic reprogramming as a pro-tumoral regulator in the tumor milieu. *Biochim Biophys. Acta Rev. Cancer* **1878**, 188962 (2023).

31. Boudhraa, Z. et al. NR1D1 regulation by Ran GTPase via miR4472 identifies an essential vulnerability linked to aneuploidy in ovarian cancer. *Oncogene* **41**, 309–320 (2022).

32. Wang, J. et al. Fucoxanthin inhibits gastric cancer lymphangiogenesis and metastasis by regulating Ran expression. *Phytomedicine* **118**, 154926 (2023).

33. Bannoura, S. F. et al. RCC1 regulation of subcellular protein localization via Ran GTPase drives pancreatic ductal adenocarcinoma growth. *Cancer Lett.* **604**, 217275 (2024).

34. Wang, K. et al. Targeting the GTPase RAN by liposome delivery for tackling cancer stemness-emanated therapeutic resistance. *J. Control Release* **375**, 589–600 (2024).

35. Gao, W. et al. Up-regulation of RAN by MYBL2 maintains osteosarcoma cancer stem-like cells population during heterogeneous tumor generation. *Cancer Lett.* **586**, 216708 (2024).

36. Galiger, C. et al. The survivin-ran inhibitor LLP-3 decreases oxidative phosphorylation, glycolysis and growth of neuroblastoma cells. *BMC Cancer* **23**, 1148 (2023).

37. Han, R. et al. Osimertinib in combination with anti-angiogenesis therapy presents a promising option for osimertinib-resistant non-small cell lung cancer. *BMC Med.* **22**, 174 (2024).

38. Han, F., Wang, X. & Wang, Z. Molecular characterization of a Ran isoform gene up-regulated in shrimp immunity. *Gene* **495**, 65–71 (2012).

39. Ye, T. & Zhang, X. Involvement of Ran in the regulation of phagocytosis against virus infection in S2 cells. *Dev. Comp. Immunol.* **41**, 491–497 (2013).

40. Qiao, X. et al. Ran overexpression leads to diminished T cell responses and selectively modulates nuclear levels of c-Jun and c-Fos. *J. Biol. Chem.* **285**, 5488–5496 (2010).

41. Che, X. et al. RAN and YBX1 are required for cell proliferation and IL-4 expression and linked to poor prognosis in oral squamous cell carcinoma. *Exp. Cell Res.* **406**, 112767 (2021).

42. Yang, Y. et al. Nuclear transport proteins: structure, function, and disease relevance. *Signal Transduct. Target Ther.* **8**, 425 (2023).

43. Vergote, I. et al. ENGOT-EN20/GOG-3083/XPORT-EC-042 - A phase III, randomized, placebo-controlled, double-blind, multicenter trial of selinexor in maintenance therapy after systemic therapy for patients with p53 wild-type, advanced, or recurrent endometrial carcinoma: rationale, methods, and trial design. *Int J. Gynecol. Cancer* **34**, 1283–1289 (2024).

44. Gonzalez-Calle, V. et al. Selinexor, daratumumab, bortezomib and dexamethasone for the treatment of patients with relapsed or refractory multiple myeloma: results of the phase II, nonrandomized, multicenter GEM-SELIBORDARA study. *Haematologica* **109**, 2219–2228 (2024).

45. Vergote, I. et al. Oral Selinexor as Maintenance Therapy After First-Line Chemotherapy for Advanced or Recurrent Endometrial Cancer. *J. Clin. Oncol.* **41**, 5400–5410 (2023).

46. Shimosato, Y. et al. NPM1-fusion proteins promote myeloid leukemogenesis through XPO1-dependent HOX activation. *Leukemia*. https://doi.org/10.1038/s41375-024-02438-w (2024).

47. Quintanal-Villalonga, A. et al. Inhibition of XPO1 Sensitizes Small Cell Lung Cancer to First- and Second-Line Chemotherapy. *Cancer Res.* **82**, 472–483 (2022).

48. Daneshmandi, S. et al. Exportin 1 governs the immunosuppressive functions of myeloid-derived suppressor cells in tumors through ERK1/2 nuclear export. *Cell Mol. Immunol.* **21**, 873–891 (2024).

49. Altan, M. et al. Safety, tolerability, and clinical activity of selinexor in combination with pembrolizumab in treatment of metastatic non-small cell lung cancer. *Cancer* **129**, 2685–2693 (2023).

50. Seydel, C. Single-cell metabolomics hits its stride. *Nat. Methods* **18**, 1452–1456 (2021).

51. Hu, J. et al. Tumor microenvironment remodeling after neoadjuvant immunotherapy in non-small cell lung cancer revealed by single-cell RNA sequencing. *Genome Med.* **15**, 14 (2023).

52. Kim, N. et al. Single-cell RNA sequencing demonstrates the molecular and cellular reprogramming of metastatic lung adenocarcinoma. *Nat. Commun.* **11**, 2285 (2020).

53. Wu, Y. et al. Spatiotemporal Immune Landscape of Colorectal Cancer Liver Metastasis at Single-Cell Level. *Cancer Discov.* **12**, 134–153 (2022).

54. Charoentong, P. et al. Pan-cancer Immunogenomic Analyses Reveal Genotype-Immunophenotype Relationships and Predictors of Response to Checkpoint Blockade. *Cell Rep.* **18**, 248–262 (2017).

55. Jiang, P. et al. Signatures of T cell dysfunction and exclusion predict cancer immunotherapy response. *Nat. Med.* **24**, 1550–1558 (2018).
56. Liang, R. Letter to the editor regarding "XPO1 inhibition synergizes with PARP1 inhibition in small cell lung cancer by targeting nuclear transport of FOXO3a. *Cancer Lett.* **524**, 193 (2022).
57. Wang, J. et al. Exosomal miR-27a Derived from Gastric Cancer Cells Regulates the Transformation of Fibroblasts into Cancer-Associated Fibroblasts. *Cell Physiol. Biochem.* **49**, 869–883 (2018).
58. Detre, S., Saclani Jotti, G. & Dowsett, M. A "quickscore" method for immunohistochemical semiquantitation: validation for oestrogen receptor in breast carcinomas. *J. Clin. Pathol.* **48**, 876–878 (1995).

Author contributions
Q.D., R.L. and J.W. contributed equally to this study. Q.D., D.H., and T.Q. conceived and designed the study. QD, R.L. and J.W. performed the formal analysis. Q.D., J.W., Y.J., and Q.X. collected the samples and clinical information. Q.D., T.Q., R.L., and J.W. performed the cell and mice experiments. Q.D., and T.Q. drafted the manuscript. All authors critically revised the manuscript. All authors read and approved the final manuscript.

Competing interests
The authors declare no competing interests.

Additional information
Supplementary information The online version contains supplementary material available at https://doi.org/10.1038/s41698-025-00977-8.

Correspondence and requests for materials should be addressed to Dingzhi Huang or Tingting Qin.

Reprints and permissions information is available at http://www.nature.com/reprints

Publisher's note Springer Nature remains neutral with regard to jurisdictional claims in published maps and institutional affiliations.